ELSEVIER

International Journal of Solids and Structures 41 (2004) 1879–1892

INTERNATIONAL JOURNAL OF SOLIDS and STRUCTURES

www.elsevier.com/locate/ijsolstr

Dynamic behavior of folded composite plates analyzed by the third order plate theory

Sang-Youl Lee [a], Shi-Chang Wooh [a,*], Sung-Soon Yhim [b]

[a] *Department of Civil and Environmental Engineering, Massachusetts Institute of Technology, 77 Massachusetts Avenue, Cambridge, MA 02139, USA*

[b] *Department of Civil Engineering, University of Seoul, 90 Junneoung-Dong, Dongdaemoon-Gu, Seoul 130-743, South Korea*

Received 19 May 2003; received in revised form 11 November 2003

Abstract

This study investigates the dynamic behavior of multiply-folded composite laminates analyzed the high order plate theory. Using the third order finite element program developed for this study, the effects of folding angles and ply orientations on the transient responses for various loading and boundary conditions are studied. The numerical results obtained are in good agreement with those reported by other investigators. Furthermore, the new results reported in this paper show the interactions between folding angels and layup sequences. Key observation points are discussed and a brief design guideline is given.

Keywords: Composite materials; Folded plates; Finite element analysis; Third order plate theory; Dynamic responses; Folding angles

1. Introduction

The abundance of folded plate members offers a broad range of structural engineering applications such as culverts, ship hulls, buildings, and box girder bridges. With the advancement of technology in fiber-reinforced composite materials, the applicability of composites to such members has been increased significantly due to their merits such as low density, high stiffnesses and high strengths.

Structural behavior of folded isotropic plates has been studied previously by a host of investigators using a variety of approaches. Goldberg and Leve (1957) developed a method based on elasticity, which was subsequently modified and applied by De Fries-Skene and Scordelis (1964). The methods in this category are common because of their superb computational accuracy. However, it is difficult to apply these methods directly to folded plates or to dynamic problems, so that they have been extended by other investigators to deal with those problems. For example, Scordelis (1966) and Chu and Dudnik (1969) analyzed simply supported box bridges using a similar technique. Cheung (1969) introduced the finite strip method for

* Corresponding author. Tel.: +1-617-253-7134; fax: +1-617-253-6044.
E-mail addresses: scwooh@mit.edu, scwooh@hotmail.com (S.-C. Wooh).

0020-7683/$ - see front matter © 2003 Elsevier Ltd. All rights reserved.
doi:10.1016/j.ijsolstr.2003.11.026

analyzing folded prismatic plates and box girders. Liu and Huang (1992) solved the problems for one- and two-folded plates using a finite element transfer matrix method. Zienkiewicz and Taylor (2000) presented a flat shell technique which can be applied directly to folded plates. Dynamic problems are also tackled by many investigators. For example, Irie et al. (1984) calculated the natural frequencies of folded cantilever plates using the Ritz method. Danial et al. (1996) introduced a concept referred to as spectral element method. Lee et al. (2002) analyzed the dynamic response of a prestressed concrete box girder bridge subjected to moving loads using folded plate elements.

All these works are limited, in that they can analyze only the structural members made of isotropic materials. Recently, techniques for analyzing anisotropic plates are evolved. Suresh and Malhotra (1998) studied the free vibration of damped composite box beams using four node plate elements with five degrees of freedom (DOF) per node. Niyogi et al. (1999) carried out a finite element vibration analysis of folded laminates using a first order plate theory, often referred to as the FOPT. In general, a first order shear deformation theory can describe easily and accurately the kinematic behavior of a flat composite plate (Reddy, 1997). However, it requires an estimation of shear correction factors; a value of $K = 5/6$ is normally used (Khdeir and Reddy, 1991). On the other hand, the third order shear deformation theory (TSDT) is free from such requirements and thus can yield more accurate results for both static and dynamic conditions than those of the first order theories. This allows for convenient use of high order plate theory (HOPT). Many high order theories exist but they are mostly applicable to unfolded (flat) isotropic or anisotropic plates at the present time (Krishna, 1977; Bhimaraddi and Stevens, 1984; Reddy and Phan, 1985; Murthy, 1981; Kant et al., 1990).

Lee and Wooh (2003) extended the theory to study free vibration of composite box beams using the FEM, in which they demonstrated the criticality of the HOPT in analyzing folded structures. For a folded composite laminate, the folding angles and layup sequences could play a dominant role in determining the dynamic characteristics. Thus, the study is further extended in this investigation to take into account the effects of folding angles and stacking sequences. The focus is on forced vibration and different boundary conditions. To obtain the results coupled with complicated nonlinear behavior, this study uses the HOPT.

2. Theoretical formulation

The HOPT used to analyze unfolded laminates reviewed in this study is derived from the third-order laminate formulation (Reddy, 1997). The theory is based on the same assumptions as those of the classical and FOPTs, except that we no longer assume that the straight lines normal to the middle surface remain straight after deformation but it is assumed that they can be expressed in the form of a cubic equation.

2.1. Finite element formulation for HOPT

For completeness, the shear deformation theory and the relevant formulas in the finite element analysis of flat plates are reviewed below. A nonconforming element for unfolded plates have 7-DOF per node, that is, the mid-plane displacements in the x-, y-, and z-directions (u_0, v_0, w_0), the respective derivatives ($w_{0,x}$, $w_{0,y}$), and the rotations (ϕ_x, ϕ_y). The generalized displacements can be approximated over an element Ω^e by the expressions

$$\begin{Bmatrix} u_0 \\ v_0 \\ \phi_x \\ \phi_y \end{Bmatrix} = \sum_{j=1}^{4} \Psi_j [I_2] \begin{Bmatrix} u_{0j} \\ v_{0j} \\ \phi_{xj} \\ \phi_{yj} \end{Bmatrix} \quad \text{and} \quad \begin{Bmatrix} w_0 \\ w_{0,x} \\ w_{0,y} \end{Bmatrix} = \sum_{j=1}^{4} \begin{bmatrix} \Phi_j & \Phi_j & \Phi_j \\ \Phi_{j,x} & \Phi_{j,x} & \Phi_{j,x} \\ \Phi_{j,y} & \Phi_{j,y} & \Phi_{j,y} \end{bmatrix} \begin{Bmatrix} w_{0j} \\ w_{0j,x} \\ w_{0j,y} \end{Bmatrix}, \tag{1}$$

where $[I_2]$ is a 2×2 identity matrix, Ψ_j are the Lagrange interpolation functions and Φ_j, $\Phi_{j,x}$ and $\Phi_{j,y}$ are the Hermite interpolation functions, and their first derivatives, respectively. For the third plate theory, the following relationship is valid:

$$\begin{aligned} u(x,y,z,t) &= u_0(x,y,t) + z\phi_x(x,y,t) - c_1 z^3(\phi_x + c_0 w_{0,x}),\\ v(x,y,z,t) &= v_0(x,y,t) + z\phi_y(x,y,t) - c_1 z^3\left(\phi_y + c_0 w_{0,y}\right),\\ w(x,y,z,t) &= w_0(x,y,z,t), \end{aligned} \tag{2}$$

where c_0 and c_1 are the parameters referred to as *tracers*. The condition $c_0 = 1$, $\phi_x = -w_{0,x}$ and $\phi_y = -w_{0,y}$ in Eq. (2) yields the same displacement field as that of the classical lamination theory (CLT). The displacement field becomes identical to that of FOPT for $c_1 = 0$. Note that $c_0 = 1$ for HOPT which is our case.

2.2. Plate element stiffness matrix

The stiffness matrix $[K_e]$ of a plate element is assumed to be

$$[K]_e = \int_0^a \int_0^b [B]^{\mathrm{T}}[D][B]\,\mathrm{d}x\,\mathrm{d}y, \tag{3}$$

where a and b are the dimensions of a rectangular plate, $[B]$ is the strain–displacement matrix, and $[D]$ is a stiffness matrix in the global coordinates. Alternatively, Eq. (3) can be rewritten in the natural coordinates (ξ, η) as

$$[K]_r = \int_{-1}^{1}\int_{-1}^{1} [\overline{B}]^{\mathrm{T}}[D][\overline{B}]|J|\,\mathrm{d}\xi\,\mathrm{d}\eta, \tag{4}$$

where $|J|$ is the determinant of Jacobian matrix. The 13×28 strain–displacement matrix $[\overline{B}]$ in the (ξ, η) coordinates is given by

$$[\overline{B}] = \sum_{j=1}^{4} \begin{bmatrix} \Psi_{j,\xi} & 0 & 0 & 0 & 0 & 0 & 0\\ 0 & \Psi_{j,\eta} & 0 & 0 & 0 & 0 & 0\\ \Psi_{j,\xi} & \Psi_{j,\eta} & 0 & 0 & 0 & 0 & 0\\ 0 & 0 & 0 & 0 & 0 & \Psi_{j,\xi} & 0\\ 0 & 0 & 0 & 0 & 0 & 0 & \Psi_{j,\eta}\\ 0 & 0 & 0 & 0 & 0 & \Psi_{j,\xi} & \Psi_{j,\eta}\\ 0 & 0 & -c_1\Phi_{j,\xi\xi} & -c_1\Phi'_{j,\xi\xi} & -c_1\Phi''_{j,\xi\xi} & -c_1\Psi_{j,\xi} & 0\\ 0 & 0 & -c_1\Phi_{j,\eta\eta} & -c_1\Phi'_{j,\eta\eta} & -c_1\Phi''_{j,\eta\eta} & 0 & -c_1\Psi_{j,\eta}\\ 0 & 0 & -c_1\Phi_{j,\xi\eta} & -c_1\Phi'_{j,\xi\eta} & -c_1\Phi''_{j,\xi\eta} & -c_1\Psi_{j,\xi} & -c_1\Psi_{j,\eta}\\ 0 & 0 & \Phi_{j,\eta} & 0 & 0 & 0 & \Psi_j\\ 0 & 0 & \Phi_{j,\xi} & 0 & 0 & \Psi_j & 0\\ 0 & 0 & -c_2\Phi_{j,\eta} & 0 & 0 & 0 & -c_2\Psi_j\\ 0 & 0 & -c_2\Phi_{j,\eta} & 0 & 0 & -c_2\Psi_j & 0 \end{bmatrix} \tag{5}$$

and the 13×13 stiffness matrix $[D]$ could be expressed as

$$[D]=\begin{bmatrix}
A_{11} & A_{12} & A_{16} & B_{11} & B_{12} & B_{16} & E_{11} & E_{12} & E_{16} & 0 & 0 & 0 & 0\\
A_{12} & A_{22} & A_{26} & B_{12} & B_{22} & B_{26} & E_{12} & E_{22} & E_{26} & 0 & 0 & 0 & 0\\
A_{16} & A_{26} & A_{66} & B_{16} & B_{26} & B_{66} & E_{16} & E_{26} & E_{66} & 0 & 0 & 0 & 0\\
B_{11} & B_{12} & B_{16} & D_{11} & D_{12} & D_{16} & F_{11} & F_{12} & F_{16} & 0 & 0 & 0 & 0\\
B_{12} & B_{22} & B_{26} & D_{12} & D_{22} & D_{26} & F_{12} & F_{22} & F_{26} & 0 & 0 & 0 & 0\\
B_{16} & B_{26} & B_{66} & D_{16} & D_{26} & D_{66} & F_{16} & F_{26} & F_{66} & 0 & 0 & 0 & 0\\
E_{11} & E_{12} & E_{16} & F_{11} & F_{12} & F_{16} & H_{11} & H_{12} & H_{16} & 0 & 0 & 0 & 0\\
E_{12} & E_{22} & E_{26} & F_{12} & F_{22} & F_{26} & H_{12} & H_{22} & H_{26} & 0 & 0 & 0 & 0\\
E_{16} & E_{26} & E_{66} & F_{16} & F_{26} & F_{66} & H_{16} & H_{26} & H_{66} & 0 & 0 & 0 & 0\\
0 & 0 & 0 & 0 & 0 & 0 & 0 & 0 & 0 & A_{44} & A_{45} & D_{44} & D_{45}\\
0 & 0 & 0 & 0 & 0 & 0 & 0 & 0 & 0 & A_{45} & A_{55} & D_{45} & D_{55}\\
0 & 0 & 0 & 0 & 0 & 0 & 0 & 0 & 0 & D_{44} & D_{45} & F_{44} & F_{45}\\
0 & 0 & 0 & 0 & 0 & 0 & 0 & 0 & 0 & D_{45} & D_{55} & F_{45} & F_{55}
\end{bmatrix}, \tag{6}$$

where

$$(A_{ij},B_{ij},D_{ij},E_{ij},F_{ij},H_{ij})=\sum_{k=1}^{n}\int_{z_k}^{z_{k+1}}\overline{Q}_{ij}^{(k)}(1,z,z^2,z^3,z^4,z^6)\,\mathrm{d}z,\quad i,j=1,2,6, \tag{7}$$

$$(A_{ij},D_{ij},F_{ij})=\sum_{k=1}^{n}\int_{z_k}^{z_{k+1}}\overline{Q}_{ij}^{(k)}(1,z^2,z^6)\,\mathrm{d}z,\quad i,j=4,5. \tag{8}$$

Here, $\overline{Q}_{ij}^{(k)}$ denotes the stiffnesses of the kth layer and the positions of the top and bottom faces of the kth layer z_{k+1} and z_k.

2.3. Plate element mass matrix

The equations of motion for the laminated composite plate based on the third order theory can be written as follows:

$$\begin{aligned}
&N_{xx,x}+N_{xy,y}=I_0\ddot{u}_0+J_1\ddot{\phi}_x-c_1I_3\ddot{w}_{0,x},\\
&N_{xy,x}+N_{yy,y}=I_0\ddot{v}_0+J_1\ddot{\phi}_y-c_1I_3\ddot{w}_{0,y},\\
&\overline{Q}_{x,x}+\overline{Q}_{y,y}+c_1(P_{xx,xx}+2P_{xy,xy}+P_{yy,yy})+F\\
&\quad=I_0\ddot{w}_0-c_1^2I_6(\ddot{w}_{0,xx}+\ddot{w}_{0,yy})+c_1\left[I_3(\ddot{u}_{0,x}+\ddot{v}_{0,y})+J_4(\ddot{\phi}_{x,x}+\ddot{\phi}_{y,y})\right],\\
&\overline{M}_{xx,x}+\overline{M}_{xy,y}-\overline{Q}_x=J_1\ddot{u}_0+K_2\ddot{\phi}_x-c_1J_4\ddot{w}_{0,x},\\
&\overline{M}_{xy,x}+\overline{M}_{yy,y}-\overline{Q}_y=J_1\ddot{v}_0+K_2\ddot{\phi}_y-c_1J_4\ddot{w}_{0,y},
\end{aligned} \tag{9}$$

where N_{xx}, N_{yy}, and N_{xy} are the normal and shear force resultants, $\overline{M}_{xx}$, $\overline{M}_{yy}$, and $\overline{M}_{xy}$ are the moment resultants, $\overline{Q}_x$ and $\overline{Q}_y$ are the transverse force resultants, F is the distributed load, and

$$\overline{M}_{\alpha\beta}=M_{\alpha\beta}-c_1P_{\alpha\beta},\quad \overline{Q}_\alpha=Q_\alpha-c_2R_\alpha, \tag{10}$$

$$I_i=\sum_{k=1}^{m}\int_{z_k}^{z_{k+1}}\rho^{(k)}z^i\,\mathrm{d}z\quad(i=0,1,2,\ldots,6), \tag{11}$$

$$J_i=I_i-c_1I_{i+2},\quad K_2=I_2-2c_1I_4+c_1^2I_6,\quad c_1=\frac{4}{3h^2},\quad c_2=3c_1, \tag{12}$$

where m is the total number of layers, $\rho^{(k)}$ is the mass density of the kth layer, h is the wall thickness, and (P_{xx}, P_{yy}, P_{xy}) and (R_x, R_y) denote the higher order resultants respectively given as

$$\begin{Bmatrix} P_{xx} \\ P_{yy} \\ P_{xy} \end{Bmatrix} = \int_{-h/2}^{h/2} \begin{Bmatrix} \sigma_{xx} \\ \sigma_{yy} \\ \sigma_{xy} \end{Bmatrix} z^3 \, dz, \quad \begin{Bmatrix} R_x \\ R_y \end{Bmatrix} = \int_{-h/2}^{h/2} \begin{Bmatrix} \sigma_{yz} \\ \sigma_{xz} \end{Bmatrix} z^2 \, dz. \tag{13}$$

Eq. (9) can be rewritten in compact form as

$$\{S\} = [\mu]\{A\}, \tag{14}$$

where $\{S\}$, $[\mu]$, and $\{A\}$ are respectively the force vector, inertia matrix, and the acceleration vector. The mass matrix of the unfolded flat element is given by the relationship

$$[M]_e = \int_0^a \int_0^b [H]^{\mathrm{T}}[\mu][H] \, dx \, dy = \int_{-1}^{1} \int_{-1}^{1} [\overline{H}]^{\mathrm{T}}[\mu][\overline{H}]|J| \, d\xi \, d\eta, \tag{15}$$

where $[\overline{H}]$ is a matrix consisting of Lagrange and Hermite interpolation functions.

2.4. Folded plate elements

It is known that a global stiffness matrix is singular and ill-conditioned because of the null diagonal terms due to the drilling DOF ϕ_z in the transformed element stiffness matrix. As a result, it is not possible to obtain directly the shape function of the drilling DOF induced by transformation. To resolve this problem in a finite element analysis, we could insert an artificial in-plane rotational angle or equivalently rotational stiffness coefficients. In our analysis, we add an eighth drilling DOF to the existing 7-DOF system, as suggested by Lee et al. (2002) and Lee and Wooh (2003). The deformation of each element expressed in the local coordinates can be transformed into the loading coordinates using the following transformation relationship (see Fig. 1):

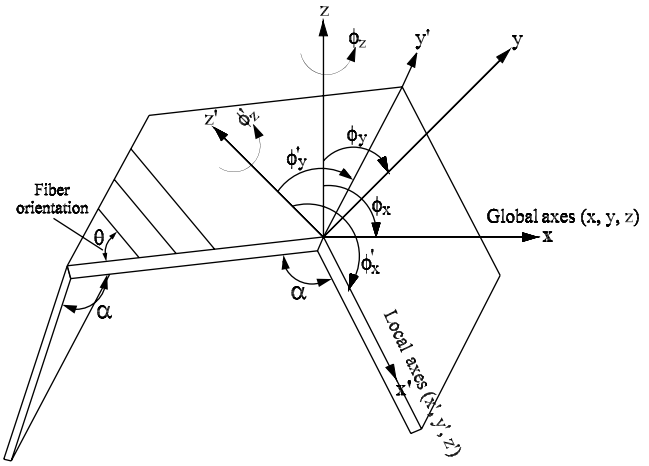

Fig. 1. Coordinate transformation of a folded plate element.

$$\begin{Bmatrix} u_0 \\ v_0 \\ w_0 \\ w_{0,x} \\ w_{0,y} \\ \phi_x \\ \phi_y \\ \phi_z \end{Bmatrix} = \begin{pmatrix} \zeta_{x'x} & \zeta_{x'y} & \zeta_{x'z} & 0 & 0 & 0 & 0 & 0 \\ \zeta_{y'x} & \zeta_{y'y} & \zeta_{y'z} & 0 & 0 & 0 & 0 & 0 \\ \zeta_{z'x} & \zeta_{z'y} & \zeta_{z'z} & 0 & 0 & 0 & 0 & 0 \\ 0 & 0 & 0 & \zeta_{y'y} & -\zeta_{y'x} & 0 & 0 & 0 \\ 0 & 0 & 0 & -\zeta_{x'y} & \zeta_{x'x} & 0 & 0 & 0 \\ 0 & 0 & 0 & 0 & 0 & \zeta_{y'y} & -\zeta_{y'x} & \zeta_{y'z} \\ 0 & 0 & 0 & 0 & 0 & -\zeta_{x'y} & \zeta_{x'x} & -\zeta_{x'z} \\ 0 & 0 & 0 & 0 & 0 & \zeta_{z'y} & -\zeta_{z'x} & \zeta_{z'z} \end{pmatrix} \begin{Bmatrix} u'_0 \\ v'_0 \\ w'_0 \\ w'_{0,x} \\ w'_{0,y} \\ \phi'_x \\ \phi'_y \\ \phi'_z \end{Bmatrix} \tag{16}$$

or in brief,

$$\{u\} = [T]\{u'\}, \tag{17}$$

where ζ_{ij} are the direction cosines between the global and local coordinates and $[T]$ is the transformation matrix. The primed notations are used to denote the properties in the local coordinates.

The global stiffness matrix is then expressed as

$$[\overline{K}] = [\overline{T}]^T [\overline{K}]'_s [\overline{T}], \tag{18}$$

where

$$[\overline{T}] = \begin{pmatrix} [T] & 0 & 0 & 0 \\ 0 & [T] & 0 & 0 \\ 0 & 0 & [T] & 0 \\ 0 & 0 & 0 & [T] \end{pmatrix}_{32\times 32}, \quad [\overline{K}]'_s = \begin{pmatrix} [K]_{\mathrm{I}} & 0 \\ 0 & [K]_{\mathrm{II}} \end{pmatrix}_{32\times 32}. \tag{19}$$

Note that $[K]_{\mathrm{I}}$ and $[K]_{\mathrm{II}}$ are the real and artificial matrices consisting of 28×28 and 4×4 elements, respectively. Before applying the transformation, the 28×28 matrix is reconstructed into a 32×32 matrix in order to accommodate the drilling DOF ϕ_z for each element. Transformation of the mass matrix is the same as that of the stiffness matrix, that is,

$$[\overline{M}] = [T]^{\mathrm{T}} [\overline{M}]'_S [T]. \tag{20}$$

The global force vector is also expressed as

$$[\overline{F}] = [T]\{f\}_e. \tag{21}$$

Neglecting the damping effect, the governing equations for the free and forced vibration problems are respectively stated as

$$\left\{[\overline{M}] - \omega^2[\overline{K}]\right\} = \{0\} \tag{22}$$

and

$$[\overline{M}]\{\ddot{U}\} + [\overline{K}]\{U\} = \{F(t)\}, \tag{23}$$

where $\{\ddot{U}\}$ and $\{U\}$ are the acceleration and displacement vectors. The impact loading function $F(t)$ is described by an ideal rectangular spike shape of width t_0 and magnitude δ_p:

$$P(t) = \begin{cases} \delta_p & \text{for } 0 < t < t_0, \\ 0 & \text{for } t > t_0. \end{cases} \tag{24}$$

In order to understand the dynamic behavior of a system, we often need to know only a few low order eigenvalues of the system. In this study, the subspace iteration method (Bathe, 1996) is adopted to extract the eigenpairs representing the low order natural frequencies. This method selects a subspace whose

dimensions, determined by the desired number of eigenvalues to be obtained, are the same as those of the entire matrix. Then, the Jacobi iteration method is carried out on the selected matrix using the Ritz's base vector as an initial vector. This method has the advantages to effective memory management and computational efficiency as compared to other methods which carry the entire matrix in the computation (Bathe, 1996). In Eq. (23), the damping effects are neglected. Newmark's implicit integration technique which uses the equilibrium conditions at time $t + \Delta t$ is adopted for the transient analysis.

3. Numerical results

It was shown from our previous study (Lee and Wooh, 2003) that the results obtained by different composite plate theories could be noticeably different even for flat plates, depending on the given boundary conditions. In order to validate the procedure described in this paper, we compare our results with those published by other investigators. The third order finite element formulation is confirmed by studying (1) the dynamic response of an unfolded plate subjected to a uniformly distributed step loading and (2) free vibration of a folded plate. Then, a two-folded E-glass/epoxy composite structure shown in Fig. 2 is analyzed to study its transient responses to (3) a concentrated step loading and (4) concentrated rectangular impulse loading. The detailed loading and edge boundary conditions as well as other numerical parameters used in this study are tabulated in Table 1, and the mechanical and physical properties of the materials are shown in Table 2. The observation points A, B, and C are the locations where the displacements (dynamic response) are evaluated.

3.1. Case I: dynamic response of an unfolded plate subjected to a uniformly distributed step loading

In order to validate the FEM code developed for forced vibration analysis, the dynamic displacement at the center of a symmetric cross-ply composite laminate made of Material II is computed and compared with the FOPT results reported by Kant et al. (1990). The plate clamped at all four edges is loaded by a Heaviside step function distributed uniformly over its upper surface, that is,

$$P(t) = \begin{cases} \delta_p & \text{for } t > 0, \\ 0 & \text{for } t < 0, \end{cases} \tag{25}$$

where the load magnitude $\delta_p = 10$ N/cm^2. The center displacement computed at every 5 μs is displayed up to 150 μs in Fig. 3(a), showing negligible difference between the HOPT and FOPT results. On the other

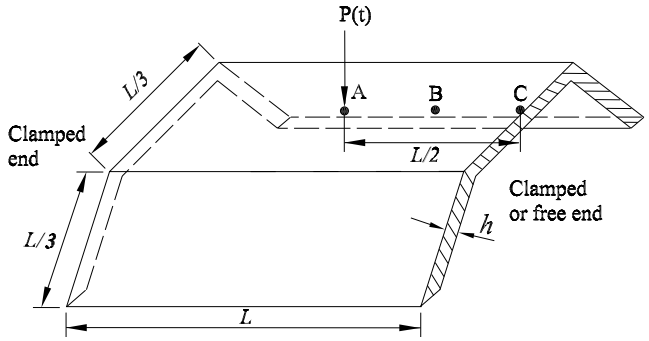

Fig. 2. Dimensions and boundary conditions of a two-folded E-glass/epoxy composite plate analyzed by the HOPT.

Table 1
Numerical parameters used in the four different case studies to demonstrate the third order finite element formulas

Parameters	Case I	Case II	Case III	Case IV
Load distribution	Uniformly distributed	n/a	Concentrated	Concentrated
Load shape	Heaviside step	n/a	Heaviside step	Rectangular step
Folding angle	Unfolded (0°)	90–150°	90–150°	120°
Layup sequences	$[0/90/0]_n$	$[45/-45/45]_n$, $[0/90]_{ns}$, $[0/90]_{2n}$, $[\pm 30]_{ns}$	$[0/90]_s$, $[\pm\theta]_{ns}$	$[45/-45/45]_n$, $[0/90]_s$, $[\pm 45]_{2n}$, $[\pm 45]_{ns}$, $[\pm\theta]_{ns}$
Material	II	I	II	II
End conditions	All clamped	Clamped–free	Clamped–free, clamped–clamped	Clamped–free
Measuring point	A	n/a	A, C	A, B, C

Table 2
Mechanical and physical properties of the materials used in this study

Material	Source	E_1	E_2	G_{12}	G_{23}	G_{13}	ν_{12}	ν_{21}	ρ
I	Niyogi et al. (1999)	60.70	24.80	12.0	12.0	12.0	0.23	0.23	1300
II	Kant et al. (1990)	$25E_2$	52.50	10.5	10.5	10.5	0.25	0.25	800

The units of E_1, E_2, G_{12}, G_{23}, G_{13} are GPa and that of ρ is kg/m^3, respectively.

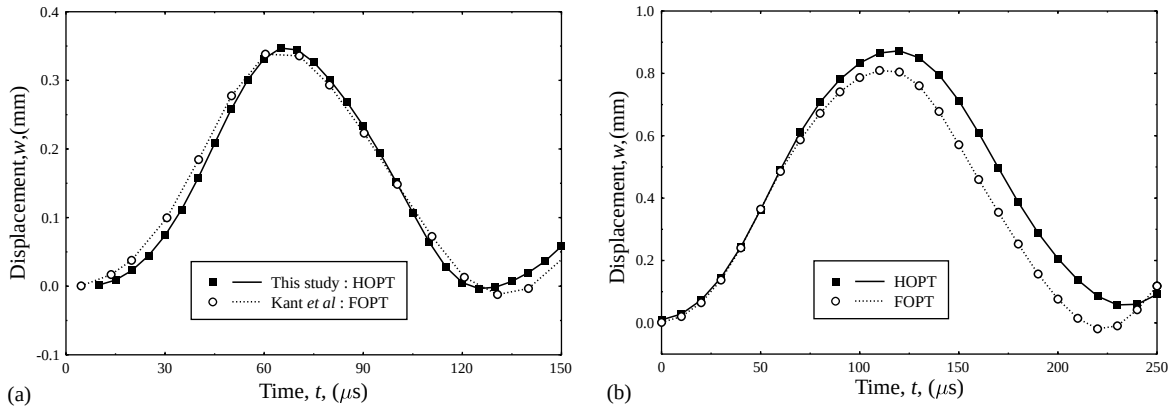

Fig. 3. Case I. Computed dynamic response of a [0/90/0] composite plate subjected to a uniformly distributed step load for different edge boundary conditions: (a) All edges are clamped. (b) One edge is clamped, all other edges are free. The displacement at the center of the plate is computed for every 5 μs.

hand, the results shown in Fig. 3(b) clearly indicate significant differences. In this case, only the boundary conditions are changed; only one of the four edges is clamped and the other edges are set free.

3.2. Case II: free vibration of a folded plate

Lee and Wooh (2003) studied the free vibration behavior of a plate folded at 90° angles using the high order theory. The analysis is extended in this study to take into account the plates with different folding angles (e.g., $\alpha = 120°$ and 150°), in which the full length $L = 2.0$ m of the plate is divided into equal folding lengths of $L/3$. The results are compared with those of Niyogi et al. (1999). They used 6×3 meshes of nine-

node quadratic elements (FOPT), while a 12×6 mesh of nonconforming elements (HOPT) is used in this study. Table 3 shows the three lowest natural frequencies for various layup sequences. It is observed that the natural frequencies obtained by the HOPT are mostly higher than those of the FOPT. In particular, the Mode 2 frequencies are different by 10–15%. Fig. 4 shows the free vibration mode shapes of a two-folded symmetric cross-ply laminate with clamped ends. As shown in the figure, some peculiar and complex mode shapes are produced due to the combined effect of both the folding angles and layup stacking sequences.

Table 3
Natural frequencies of two-folded cantilever composite plate (Material I, $L/h = 50$)

Folding angle, α	Angle orientation	Normalized frequency, $\omega = \overline{\omega}L\sqrt{\rho\frac{(1-\nu_{12}^2)}{E_1}}$					
		Niyogi et al. (FOPT)			This study (HOPT)		
		Mode 1	Mode 2	Mode 3	Mode 1	Mode 2	Mode 3
90°	$[\pm30]_{ns}$	0.0901	0.0989	0.2035	0.0925	0.1128	0.2057
	$[0/90]_{ns}$	0.0896	0.0934	0.2044	0.1055	0.1156	0.1990
	$[0/90]_{2n}$	0.0987	0.0993	0.1992	0.0982	0.1068	0.2008
	$[45/-45/45]_n$	0.0914	0.1035	0.1988	0.0897	0.1102	0.2068
120°	$[\pm30]_{ns}$	0.0781	0.0931	0.2029	0.0736	0.1096	0.2017
	$[0/90]_{ns}$	0.0761	0.0893	0.2041	0.0821	0.1132	0.1976
	$[0/90]_{2n}$	0.0772	0.0987	0.1993	0.0807	0.1027	0.1992
	$[45/-45/45]_n$	0.0745	0.0993	0.1970	0.0758	0.1038	0.2040
150°	$[\pm30]_{ns}$	0.0551	0.0869	0.1703	0.0522	0.0948	0.1595
	$[0/90]_{ns}$	0.0533	0.0840	0.1628	0.0537	0.1016	0.1760
	$[0/90]_{2n}$	0.0522	0.0906	0.1670	0.0518	0.0923	0.1634
	$[45/-45/45]_n$	0.0519	0.0898	0.1620	0.0550	0.0929	0.1649

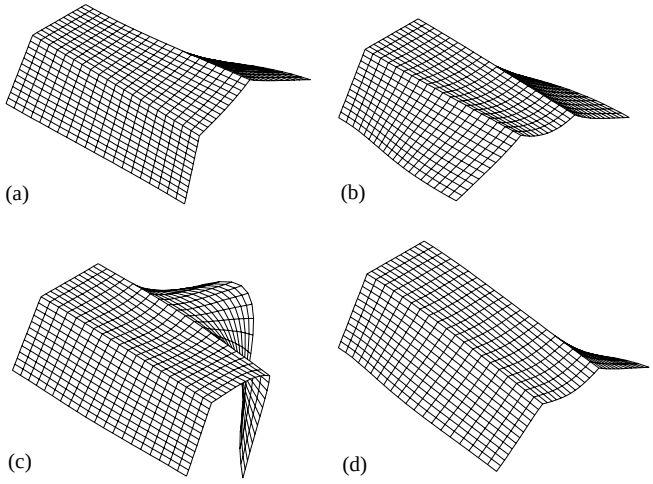

Fig. 4. Mode shapes of the lowest modes for a [0/90]$_s$ composite plate folded at ($\alpha = 150°$). (a) Mode I ($L = 20$, $L/h = 50$); (b) Mode II ($L = 20$, $L/h = 50$); (c) Mode III ($L = 20$, $L/h = 50$) and (d) Mode IV ($L = 20$, $L/h = 50$).

3.3. Case III: dynamic response of a folded plate subjected to concentrated step loading

Fig. 5 shows the dynamic displacements of a two-folded symmetric cross-ply composite plate with two different boundary conditions (clamped–free and clamped–clamped boundaries) and the folding angles ($\alpha = 90°$, 120°, and 150°). A concentrated step loading of magnitude $\delta_p = 100$ kN is applied at the center of the plate (point A) at the time $t = 0$ and the center displacement is computed at every 50 μs. For a plate with clamped–free boundaries, the displacements for the 90° and 120° folding angles are close to each other (See Fig. 5(a)). On the other hand, the induced displacement for the folding angle of 150° (which is at just the same incremental angle of 30° from 120°) is extremely higher than the others. This phenomenon makes sense to us because the flexural rigidity of the plate should decrease as the folding angle increases and it behaves nonlinearly. The difference becomes more dramatic for the case of the clamped–clamped plate shown in Fig. 5(b). We can also notice that the vibration frequency is significantly altered for the 150° folding.

Fig. 6 shows the transient displacement histories measured at point A of various angle plies folded with the fixed folding angle of 120°. The plate is subjected to a concentrated vertical step load applied at point A, and the results for various layup sequences and boundary conditions are compared. For clamped–free boundaries, the induced displacements show similar trends except that the displacement of $[\pm 60]_s$ laminate increases more rapidly in the early times (Fig. 6(a)). By contrast, the displacement amplitude of the $[\pm 60]_s$ laminate is significantly higher than the others for the clamped–clamped boundary condition (Fig. 6(b)). Furthermore, there is a significant increase of vibration frequencies when the plate edges are clamped. This observation provides us with a clue that it could be better to use small ply orientations in designing a folded angle ply especially when the boundaries are clamped. Small ply angles result in better rigidity against dynamic loading.

Fig. 7(a) shows the displacement history at point C of the same $[0/90]_s$ cross-ply laminate with clamped–free boundaries. Notice the time delays by comparing with the waveforms shown in Fig. 5. This represents the time required for the shock wave to travel the distance between the loading and detection points (points A and C). Fig. 7(b) shows the influence of ply orientations on the dynamic behavior. As the ply angle increases, the wave arrives at an earlier time and the frequency of the wave increases. This is also predictable because it is expected that a bigger ply orientation increases the stiffness in the axial direction, and consequently the wave propagation speed increases in that direction. An increased wavespeed results in

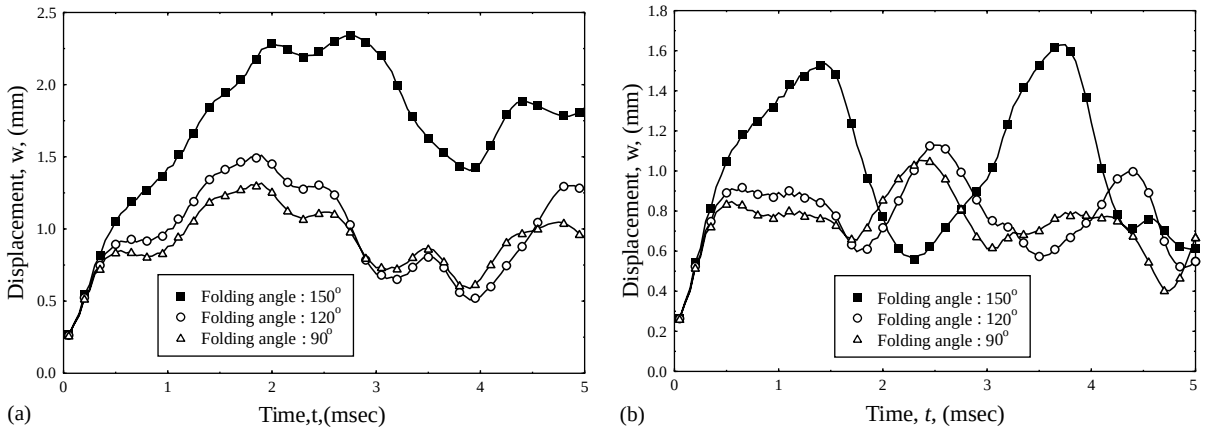

Fig. 5. Dynamic displacements of a two-folded $[0/90]_s$ laminates subjected to a step loading concentrated at point A. The clamped–free (a) and clamped–clamped (b) boundary conditions and the folding angles of 90°, 120° and 150° are considered.

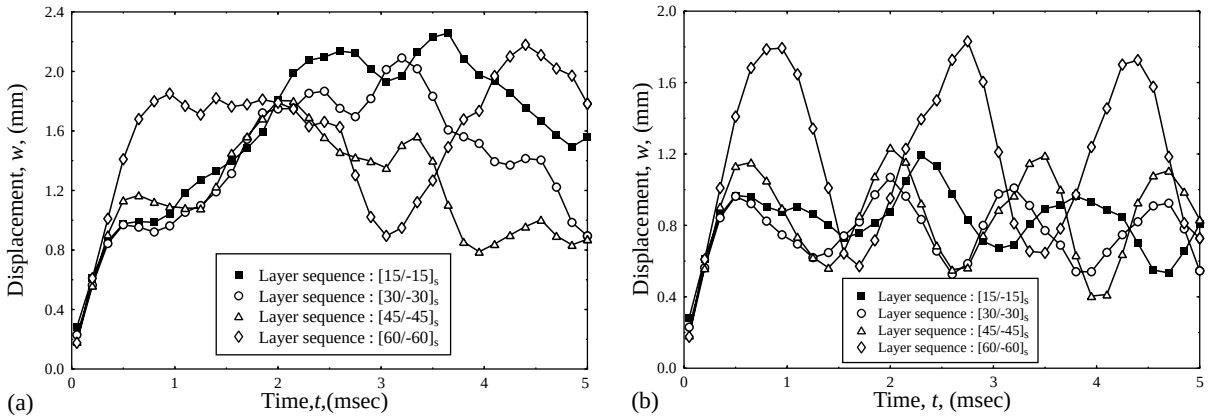

Fig. 6. Transient displacements measured at point A of angle plies folded with 120° angles. The plate is subjected to a vertical step loading concentrated at point A and the results for various layup sequences and boundary conditions are compared. (a) Clamped–free boundaries, (b) clamped–clamped boundaries.

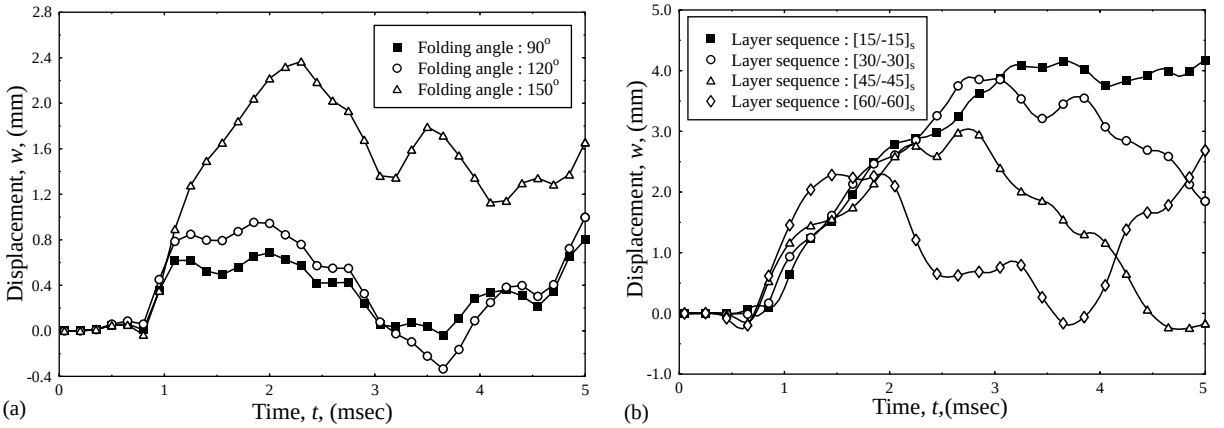

Fig. 7. Displacement history observed at point C of folded plates with clamped–free boundaries. The plate is subjected to a concentrated step load applied at point A. (a) Effect of folding angles for the $[0/90]_s$ laminate. (b) Effect of ply orientations for the 120° folding angle.

shorter arrival time and smaller wavelength. The largest displacement occurs for the laminate with the smallest ply angle, $[\pm 15]_s$, because it has the lowest bending stiffness in the lateral direction.

3.4. Case IV: dynamic response of a folded plate subjected to a concentrated rectangular pulse loading

Fig. 8 shows the dynamic responses of a folded plate subjected to a rectangular pulse (or impact) loading. A pulse of magnitude $\delta_p = 100$ kN is applied at the time $t = 0$ for the duration of 50 μs. The wave arrival times are significantly different for different layup sequences because of the same reason described earlier. On the other hand, the differences in wavespeeds due to different folding angles are negligible,

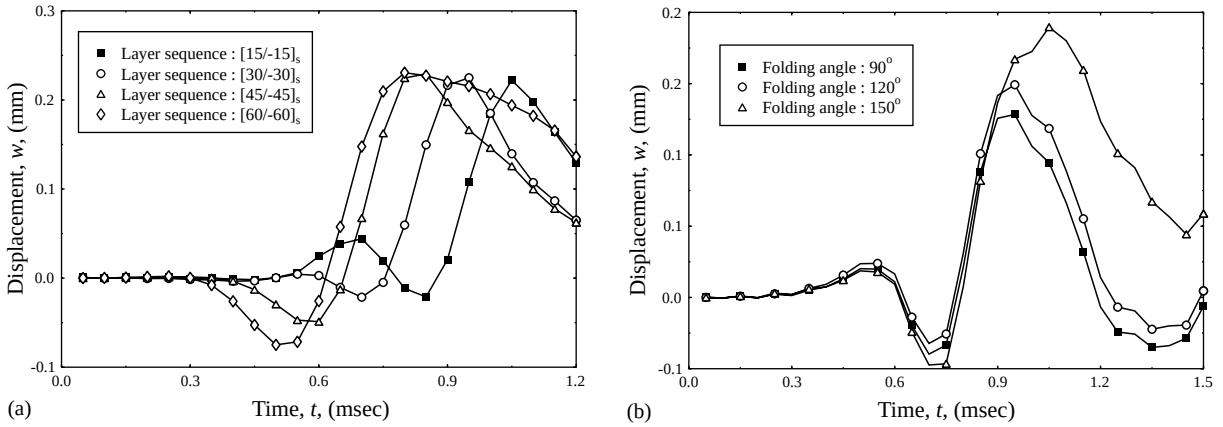

Fig. 8. Displacement history observed at point C of folded plates with clamped–free boundaries. The plate is subjected to a concentrated impact load applied at point A. (a) Effect of ply orientations for the 120° folding angle. (b) Effect of folding angles for the $[0/90]_s$ laminate.

as shown in Fig. 8(b). The folding angle of the plate makes contributions only to the displacement magnitude; the change in stiffnesses due to the folding angle is negligible so that the frequency is not greatly changed.

Table 4 shows the dynamic magnification factors (DMF) at the points A, B and C on the impact-loaded composite plate made of Material II. The DMF is defined as the ratio of displacement amplitudes of a point between its static and dynamic states. Increasing the distance between the loading and observation points raises the DMF. This is probably due to the fact that the point at far distance is under less influence by the load and freely produces higher dynamic displacement. For the folding angle of 90°, the DMF of the [±45] laminate at point A exhibits the lowest value. This stacking sequence provides the best resistance to

Table 4
Dynamic magnification factors at points A, B and C of a two-folded composite plate (Material II, $L/h = 50$, clamped–free)

Folding angle, α	Observation point	Layup sequence				
		[±45]	$[\pm 45]_s$	$[\pm 45]_2$	$[45/-45/45]_s$	$[45/-45/45]_2$
90°	A	1.441	1.442	1.527	1.449	1.480
	B	3.089	1.875	2.769	2.046	2.120
	C	4.822	2.194	3.083	2.189	2.427
105°	A	1.485	1.455	1.559	1.474	1.529
	B	2.489	1.951	2.638	1.880	2.384
	C	3.846	2.515	2.868	2.246	2.436
120°	A	1.489	1.521	1.610	1.502	1.585
	B	2.516	2.137	2.518	2.146	2.336
	C	3.567	2.601	2.982	2.285	2.553
135°	A	1.624	1.538	1.644	1.528	1.616
	B	2.477	2.010	2.225	2.039	2.133
	C	3.254	2.282	2.581	2.218	2.221
150°	A	1.653	1.497	1.512	1.481	1.482
	B	2.286	1.804	1.756	1.776	1.672
	C	2.636	2.054	1.845	1.937	1.794

dynamic loading in most conditions shown in the table. However, neither the stacking sequence nor the folding angle provides conclusive correlation with the DMF.

We can observe that the resistance of symmetric cross-ply laminates to dynamic loading is superior to that of the antisymmetric laminates. For the same number of layers, the DMF of antisymmetric laminates is always higher (or inferior dynamic resistance) except for the points B and C with the folding angle of 150°; for example, compare $[\pm 45]_s$ (symmetric) vs. $[\pm 45]_2$ (antisymmetric) or $[45/-45/45]_s$ vs. $[45/-45/45]_2$. It is easy to understand that the coupling stiffnesses B_{ij} and E_{ij} in Eq. (7), which become nonzero for antisymmetric laminates, make deleterious contributions to the dynamic behavior of the structural system.

4. Summary and conclusion

An intuitive prediction of the dynamic behavior of folded composite structures is difficult because of their complexity due to the combined effect of anisotropy and folding geometry. In this study, the dynamic characteristics are analyzed by considering various parameters. The advanced transient vibration analysis based on the third order plate theory shows the significance of stacking sequences and loading conditions for composite plates folded with arbitrary folding angles.

The parametric case studies reveal the importance of layup sequences and folding angles for efficient and economic design. We find the following key observations in designing two-folded composite structures:

1. The dynamic characteristics of flat plates analyzed by HOPT and FOPT are significant different with each other for different boundary conditions. It is especially true for clamped–free boundaries. The boundary conditions make greater contributions on the responses of folded plates for higher ply angles. In specific, the [±60] angle-ply laminate is very sensitive to the boundaries. Therefore, it is desirable to use small fiber orientations (15–45°), especially for the folding angles of 90–120°.
2. As the ply angle increases, the wave travels faster and the frequency of the wave increases due to the increased stiffness in the axial direction. On the other hand, the differences in wavespeeds due to different folding angles are negligible, because the folding angle of the plate makes contributions only to the displacement magnitude.
3. Due to the effect of the coupling stiffnesses B_{ij} and E_{ij}, the resistance of symmetric cross-ply laminates to dynamic loading is superior to that of the antisymmetric laminates.
4. We find that the usage of 150° folding angle should be avoided for almost all conditions because of its undesirable dynamic response.

The results of this study may serve as a benchmark for future guidelines in designing folded composite structures. But our parametric study is only an example and more studies should be carried out for individual design cases.

References

Bathe, K.J., 1996. The Finite Element Procedures in Engineering Analysis. Prentice-Hall, New Jersey.

Bhimaraddi, A., Stevens, L.K., 1984. A high order theory for free vibration of orthotropic, homogeneous and laminated rectangular plates. J. Appl. Mech. 51, 195–198.

Cheung, Y.K., 1969. Folded plate structures by finite strip method. J. Struct. Eng. ASCE 95, 2963–2979.

Chu, K.H., Dudnik, E., 1969. Concrete box girder bridges analyzed as folded plates. In: Concrete Bridge Design, SP-23. ACI Publications, pp. 221–246.

Danial, A.N., Doyle, J.F., Rizzi, S.A., 1996. Dynamic analysis of folded plate structures. J. Vib. Acoust. 118, 591–598.

De Fries-Skene, A., Scordelis, A.C., 1964. Direct stiffness solution for folded plates. J. Struct. Eng. ASCE 90, 15–47.

Goldberg, J.E., Leve, H.L., 1957. Theory of prismatic folded plate structures. J. IABSE 17, 59–86.
Irie, T., Yamada, G., Kobayashi, Y., 1984. Free vibration of a cantilever folded plate. J. Acoust. Soc. Am. 76, 1743–1748.
Kant, T., Varaiya, J.H., Arora, C.P., 1990. Finite element transient analysis of composite and sandwich plates based on a refined theory and implicit time integration schemes. Comp. Struct. 36 (3), 401–420.
Khdeir, A.A., Reddy, J.N., 1991. Analytical solutions of refined plate theories of cross-ply composite laminates. J. Pressure Vessel Technol. 113, 570–578.
Krishna, M.A.V., 1977. Higher order theory for vibration of thick plates. Am. Inst. Aeronaut. Astronaut. J. 15, 1823–1824.
Lee, R.C., Lee, S.Y., Yhim, S.S., 2002. A study on the dynamic responses of PSC box girder bridge under the moving load. In: Proceedings of the First International Conference on Bridge Maintenance Safety and Management, Spain.
Lee, S.Y., Wooh, S.C., 2003. Finite element vibration analysis of composite box structures using the high order plate theory. J. Sound Vib., in press.
Liu, W.H., Huang, C.C., 1992. Vibration analysis of folded plates. J. Sound Vib. 157, 123–137.
Murthy, M.V.V., 1981. An improved transverse shear deformation theory for laminated anisotropic plates. NASA Technical paper 1903, pp. 1–37.
Niyogi, A.G., Laha, M.K., Sinha, P.K., 1999. Finite element vibration analysis of laminated composite folded plate structures. J. Shock Vib. 6, 273–283.
Reddy, J.N., Phan, N.D., 1985. Stability and vibration of isotropic, orthotropic, and laminated plates according to a higher-order shear deformation theory. J. Sound. Vib. 98, 157–170.
Reddy, J.N., 1997. Mechanics of Laminated Composite Plates: Theory and Analysis. CRC Press, New York.
Scordelis, A.C., 1966. Analysis of simply supported box girder bridges. Struct. Eng. Struct. Mech. Report, University of California, Berkeley, SESM 66-17.
Suresh, R., Malhotra, S.K., 1998. Vibration and damping analysis of thin-walled box beams. J. Sound Vib. 215, 201–210.
Zienkiewicz, O.C., Taylor, R.L., 2000. The Finite Element Method Volume II: Solid Mechanics. B.H. Publications, Oxford. pp. 225–243.